Tuning the Hematite (110) Surface Properties to Enhance Its Efficiency in Photoelectrochemistry

Agata Podsiadły-Paszkowska,[†] Ionut Tranca,[‡] and Bartłomiej M. Szyja[*,†]

†*Division of Fuels Chemistry and Technology, Faculty of Chemistry, Wrocław University of Science and Technology, Gdańska 7/9, 50-344 Wrocław, Poland*

‡*Department of Mechanical Engineering, Eindhoven University of Technology, PO Box 513, 5600MB Eindhoven, The Netherlands*

E-mail: b.m.szyja@pwr.edu.pl

Abstract

We present the analysis of the role of the substitutional doping on the electronic structure of Fe_2O_3 (hematite) (110) surface. The presence of a heteroatom in different crystallographic positions in the surface layer of hematite influences the band structure – additional donor or acceptor states appear in the band gap depending on the type and charge of the heteroatom. The modifications play a role in altering the absorption coefficient, however to a minor extent in the visible light range. On the other hand, all investigated substitutions seem advantageous for the oxygen evolution reaction, as for this reaction the vacuum potential is located inside the band gap. Additionally, the differences in partial charges and binding energy suggest that the substitution site can play a role in preferential binding of the reaction intermediates.

Introduction

Photoelectrochemical (PEC)[1] water-splitting is an elegant solution to the problem of growing energy demand.[2,3] Regardless if the hydrogen obtained this way is to be used directly as a fuel, or as the reducing agent in chemical processes, PEC process allows one to utilize a clean energy and minimize the negative impact on the natural environment. In addition to being environmentally friendly, it is a relatively cheap method for hydrogen production.

As water is transparent to visible light, it is not possible to break down its molecules directly, instead a photocatalyst is required. Commonly used here are the surfaces of the semiconductors, that generate required redox potential upon the illumination. The first report of the application of this method was by Fujishima and Honda in 1972[4] and triggered a wide discussion not only on solar energy harvesting and electrocatalytic water-splitting[5–7] but also on hydrogen storage.[8]

α-Fe_2O_3 (hematite) is one of the most commonly considered materials to be used as a photoelectrode in PEC hydrogen production. It is cheap, abundant, non-toxic and chemically stable in aqueous solution of a wide range of pH. It also exhibits a proper width of the band gap: 1.9-2.2 eV,[9–12] making it capable to harvest ca. 30-37% of solar photons.[13] Although the width of the band gap of hematite is appropriate for the visible light range,[14] efficiency of this material is limited due to indirect character of this gap. An ideal material should be a direct band gap semiconductor as it makes the optical transition much easier and for that reason more efficient.[15]

Despite intensive research, the hematite-based devices have not yet achieved the theoretically predicted efficiency of 12.7-16.8%.[16] The main drawback of hematite is its electronic structure with flat bands around the band gap,[17] which results in very poor conductivity. This means that the electron-hole pairs produced under influence of light recombine quickly. Changing the nature of energy bands and improving conductivity without changing the chemical composition of the material is challenging and requires the use of nanostructures.[16,18] Unfortunately, investigation of nanostructurization is demanding experimentally

as well as computationally. It requires large unit cells to be used in calculations, which drastically increases the demand for computing power and time. The ability to perform such calculations is significantly limited making nanostructurization fairly unpredictable.

Another important possibility to alter the optical properties is doping of pure oxide material with heteroatoms.[19] The doping results in direct modification of the electronic structure of the oxide, and depending on the factors such as the ionic radius or oxidation state can have a significant influence on the resulting redox properties.[20]

Many recent computational studies focus on the bulk hematite properties and doping in the bulk geometry. Arguably, the most important modification of hematite is sulfur doping reported by Xia et al.[21] They show that sulfur doping significantly lowers the band gap width, and sulfur concentration of 5.6% improves the properties of the hematite by making a band gap direct. What is more, the modified hematite exhibit the ideal band gap width for solar light harvesting – approximately 1.45 eV. Although this result is very promising, it should be noted that doping alone can not overcome the main problem of hematite, i.e. the bands around the energy gap remain flat.

In addition to doping by the anionic sulfur, the doping at the cationic sites has been studied as well. Kosa et al. reported a combined theoretical and experimental study on Mg doping.[22] They show that Mg doping of different concentration has no significant effect on the band gap and despite the difference in the oxidation state, the system shows no introduction of holes. They ascribe it to similar effective partial charge on Mg and Fe atoms. Huda et al.[23] tried to modify the hematite band structure by transition metals (Sc, Ti, Cr, Mn, Ni) doping. They conclude that valence and conduction bands edges are modified leading to reduction of the effective mass, but this reduction is negligible. On the other hand, Ti doping of hematite leads to half-metallic band-structure. They also conclude that doping of all the used transition metals atoms except Sc leads to reduction of the unit cell volume, which affects hopping probability of localized charge carriers.

While this provides an important insight into the efficiency of the process, it needs to

be remembered, that the PEC processes occur on a semiconductor surface. Thus, the surface effects should be taken into account as they strongly affect the solar energy absorption and oxygen evolution reaction (OER).[24,25] The most commonly used hematite surface is the (0001) surface of the hexagonal cell, which is known to be stable in different terminations.[17,26–29]

The question of influence of the termination on efficiency of the OER process is a really non trivial one, and based on the existing evidence it can hardly be answered in general terms. Hellman[27] showed that the stability of the surface with different terminations depends on the applied potential. The major issue is that the terminations that are most stable at zero potential, are not stable under potential needed for water-splitting. Ovcharenko[29] and Huang[26] show the differences in the free energy for the surfaces with different terminations, that affect the properties of the surface, including adhesion, reactivity, and propensity to create defects. Pan[17] showed that water molecule is prone to adsorb on the defective site. On the other hand, the defects have an adverse effect on the energy barrier of water-splitting. All those effects described above complicate the selection of the model, however the detailed investigation of these effects, although intriguing, is beyond the scope of this paper.

In this paper we propose to use another model, that is (110) surface of the rhombohedral cell of hematite, as investigated by the group of Bieberle-Hütter.[30] The termination of the surface was selected to avoid artificial polarization, as this should make this termination stable, what is in agreement with experimental results.[31,32] The (110) surface of hematite has not been studied computationally very extensively.[30] We consider doping this surface with single transition metal atoms – Ti, Co and Ni. These are the elements that have already been used to dope hematite with promising results.[33–37]

It also needs to be stressed out that the model we propose is different from the ones involving bulk doping. Improving the photo-electrocatalytic system performance by bulk doping is relevant for such effects as conductivity and band gap width. However, catalysis is a surface phenomenon, and surface doping will significantly alter other aspects of photo-

electrocatalytic water splitting – for instance stability of intermediates.

This method is in line with the trend popular in recent years – using dispersed metal atoms as catalytically active sites i.e. single atom catalysis (SAC).[38] It has been shown that in many cases individual metal atoms are active catalysts, while their nanoparticles, although easier to be produced experimentally, are catalytically inactive.[39–41] Oxides are commonly used as the supports for SAC, due to the vacancies and OH groups present on their surfaces, which are able to stabilize single metal atoms.

The aim of our research is on one hand to determine the energy structure of such a hematite surface and the possible effect of doping on improving its optical properties. On the other hand, we want to estimate whether such a surface will be reactive and suitable for the OER study.

Model and computational details

The calculations were performed within Density Functional Theory (DFT) framework as implemented in the VASP[42,43] code. The exchange-correlation energy was used in the Perdew-Burke-Ernzerhof[44] form. The energy cutoff was set to 500 eV in all calculations. The electron–ion interactions were described by the projected augmented waves (PAW) method.[43,45]

The Brillouin zone (BZ) was sampled by $3 \times 2 \times 1$ k-points grid according to the Monkhorst-Pack scheme[46] for the surface optimization and by $6 \times 4 \times 1$ k-points for the calculation of the electronic properties. The slab consisted of 12 monolayers (MLs) of the 2×2 unit cell of hematite (110) surface. 8 of them were fixed at their bulk positions and 2 MLs on each border of the slab were allowed to move, making the system symmetrical to avoid any possible artificial polarization. The system was relaxed till the forces on each atom were less than 0.03 eV/Å. The bulk calculations for pure and doped hematite were done in a similar geometry, using 4ML of 2×2 (110) surface unit cell. In this calculations the BZ was sampled by a $3 \times 2 \times 2$ k-points grid for the optimization and $6 \times 4 \times 4$ k-points

for the electronic properties calculations.

In order to take into account the strong on-site Coulomb interaction we used the Hubbard U correction scheme. It is a common practice to fit the U value in a semi-empirical way, most often to the experimentally obtained band gap of the investigated material. This is frequently insufficient, as the change of the chemical environment, for instance upon doping the material may cause the need to change the U value for the atoms in this environment. Thus, applying the correct values of the U correction is very onerous, as it would even require the use of different values for the same element in different chemical environments. However, having in mind that the differences in the value of the U correction for the atoms of the same element but in different environment are not very significant – it can be assumed that in a similar material, i.e. a metal oxide, changes in the description of the electronic state of the system will be minor. In the present work we have used the following approach to select the U values: For Fe atoms the $U - J$ value was set to 4.3 eV, according to Dudarev's approach,[47] which was obtained in self-consistent calculations[48] and is known to reproduce the hematite band gap properly.[49] For the hematite surface with heteroatoms (Ti, Co or Ni) substitutions, we have kept the same 4.3 eV value for Fe. For the heteroatoms, we applied the $U - J$ correction values for Ti, Co and Ni as obtained for the oxides of these metals i.e. 10.0 eV,[50–52] 5.9 eV[53,54] and 5.77 eV,[55] respectively.

A 1×1 surface unit cell contains four nonequivalent Fe atoms. Two of them differ in the geometrical position at the surface, as they have different z-coordinate – they are referred to as the hill and the valley atoms. Both – hill and valley – can also have a different magnetic moment direction. We have examined all possible positions of the substituted atoms in this work. The positions of the substitution sites and the frozen layers are shown in Figure 1.

Binding energies of the substituted atoms were calculated according to the definition as:

$$E_b = E_0 + E_X - E_{doped}, \tag{1}$$

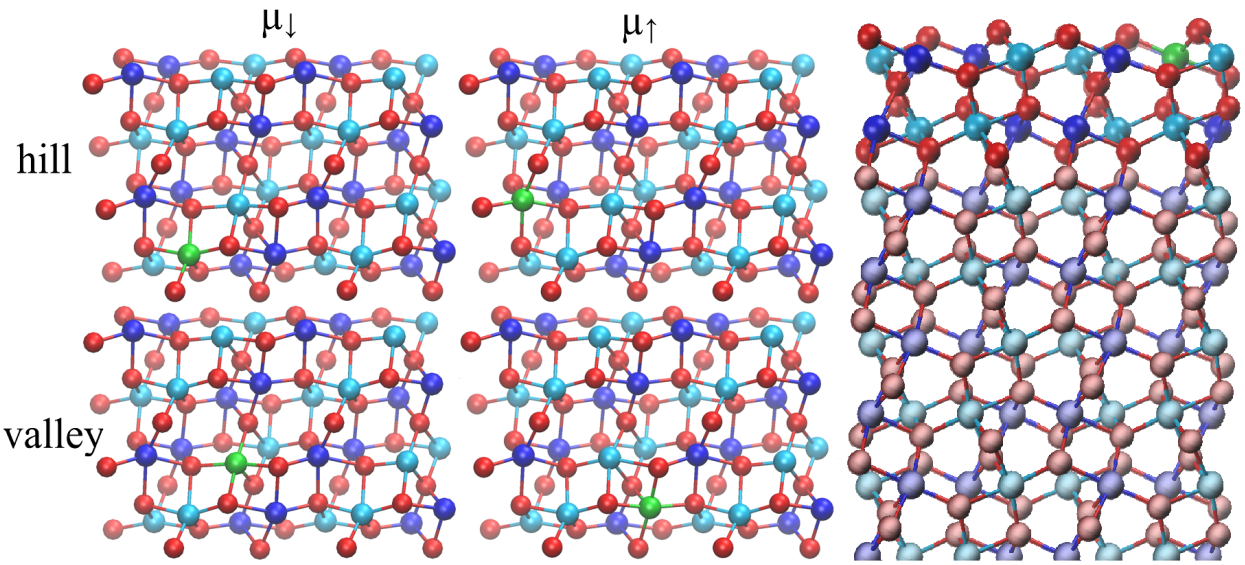

Figure 1: (left) Four different positions of the atom substitution in the unit cell (top view perspective). (right) Frozen and relaxed layers in a side view of the surface. Red, blue and cyan spheres represent oxygen and iron atoms of $\mu_\uparrow$ and $\mu_\downarrow$ respectively. The substitution site is marked by a green sphere.

where E_0, E_X and E_{doped} are the total energies of the hematite surface with a single iron vacancy, the single atom of the dopant and the doped hematite surface, respectively. Partial charges on atoms and bond orders have been calculated using the DDEC6 scheme.[56–58] We also calculated the real (ϵ_1) and imaginary (ϵ_2) parts of the dielectric function to obtain the absorption coefficient using the following equation:[59]

$$\alpha(\omega) = \sqrt{2\omega}\sqrt{\sqrt{\epsilon_1^2(\omega) + \epsilon_2^2(\omega)} - \epsilon_1(\omega)} \tag{2}$$

In order to analyze and visualize the topology of the electron density in conformity with the QTAIM theory,[60–62] an in-house written script and freely available AIM-UC software[63] were used. Bond-critical points (BCPs) were assigned to saddle-points along the bond-paths. The Laplacian at a BCP was used to characterize the nature of the pairwise interaction, providing insight into the covalent/ionic character of a bond. Using the electron density, the Laplacian and the virial theorem, the kinetic and potential electronic energy densities were also calculated. The ratio of the potential-energy density $|V_c|$ and the kinetic-energy

density G_c at the critical points provides an additional (possible more sensible) criterion for the identification of the atomic interactions. Values smaller than 1 are characteristic to ionic bonds, while values greater than 2 indicate the covalent bond. Values between 1 and 2 are characteristic for bonds having intermediate ionic/covalent characteristics.

Results and discussion

Surface model and binding energies

Hematite is an antiferromagnet with the ferromagnetic ordering in a (0001) plane and opposite direction of magnetic moments in the consecutive layers.[64] In our simulations, we have obtained a magnetic moment of the bulk Fe atoms equal to $4.2\mu_B$, which is about $0.7\mu_B$ lower then the experimental result.[65] However, due to the different method used in the present work (different functional used and different U value), we have obtained significantly better results than in the work of Rollmann et al.[49]

A characteristic feature of the (110) surface model is the different z-coordinate (perpendicular to the surface) of the Fe atoms forming the surface. They are further referred to as hill and valley regions. This is in agreement with the previous experimental results and is a characteristic feature of (110) and (012) surfaces of hematite.[32] It has to be noted, that the difference in the position of the hill and valley atoms is relatively small and amounts to 0.1 Å. In addition, this effect is only present in the surface layer – in the bulk, the z-coordinate of the Fe atoms are the same.

Despite this small difference in the z-coordinate, there are significant differences in the properties of these atoms. Thus, in the pure hematite (110) surface, the binding energy of Fe atoms amounts to 8.6 eV and 9.6 eV for valley and hill, respectively. Additionally, the partial charges of the surface Fe atoms follow a similar pattern – 1.44-1.45 e for the hill, and 1.48-1.49 e for the valley positions. These differences are the result of the surface termination, where the hill Fe atoms are missing the oxygen in their coordination spheres.

This is confirmed by the difference in the sum of bond orders (SBO) of the Fe atoms, which for all bulk and valley Fe atoms amounts to 2.62-2.68, and for surface hill atoms to 2.53.

Consequently, similar results can be observed for the heteroatoms substituting different surface Fe atoms. Table 1 shows the values of the binding energies of the substituted atoms

Table 1: Values of binding energy (in eV) of a heteroatom with different magnetic moment and position in the unit cell.

		Ti	Co	Ni
hill	$\mu_\downarrow$	2.1	2.0	0.9
	$\mu_\uparrow$	2.1	1.8	0.9
valley	$\mu_\downarrow$	1.4	0.7	0.6
	$\mu_\uparrow$	1.4	0.6	0.6

in each of the tested positions in the surface unit cell. The binding energies do not vary significantly when the heteroatom is located in a position corresponding to the Fe atom of different magnetic moment site. In fact, for Ti and Ni, the differences are below the accuracy of the DFT method. The biggest differences are observed for Co and amount to 0.2 eV and 0.1 eV for the hill and the valley sites, respectively.

On the other hand the binding energy depends strongly on the position of the heteroatom in the hill or valley location. For each atomic species the heteroatom in the hill position is bound stronger than in the valley position. This difference is approximately 0.3, 0.7 and 1.3 eV for Ni, Ti and Co, respectively. This difference is significant enough to favor the binding of the heteroatoms in the hill position. Similar difference in stability is observed for the non-substituted surface, where the difference in binding energy of the Fe atom amounts to 0.2 eV for different magnetic moment directions, and in the hill/valley position to 1.1 eV. That proves that the location of the surface atoms in the hill/valley region contributes more to the binding of a particular atom than the magnetic moment. This observation is consistent with the findings of Noerpel[31] with respect to binding of Pb atoms to the Fe_2O_3 (110) surface, although the authors attribute the differences in binding to differently coordinated sites.

The low values of binding energy of Ni atoms to the surface indicate that this kind of

doping may be difficult to be obtained experimentally. On the other hand, a different binding energy for the substitutional atom than for Fe atoms might be beneficial in formation of an active site for the interactions with the water molecules.[66–68] In fact, all of the investigated atoms bind significantly less strongly to the surface, making all of them promising candidates as co-catalysts in the water-splitting process.

Such a significant reduction in binding energy suggest a change in the bond character, however the bond orders calculated for the heteroatoms do not fully confirm this. Weak binding of the Ni atom can be explained by the SBO value higher than the optimal 2 (2.24 in hill and 2.44 in the valley position). A surface atom should have a smaller SBO due to the unsaturated coordination on one side, and the too high SBO suggests antibonding states are already occupied.

Additionally, for the hill sites, where the binding is stronger, the SBO is lower – what is in agreement with occupation of antibonding states.

The Co-substituted system displaying the biggest differences in binding for hill/valley configurations, shows only small differences in binding. The values of SBO amount to 2.4 and 2.6 for the valley and hill, respectively, and they are greater than optimal value of 2. However, the Co atoms in the hill configuration are oxidized to +3 (more discussion in the DOS section), and this implies the optimal value of SBO should be 3. The smaller value obtained is a result of the undercoordination on the surface. Similarly to the Ni case, the Co in the valley configuration

This is supported by the individual bonds strength of the Co in the hill configuration – the strongest Co-O bond has the order of 0.82, whereas the Ni and Ti bonds with oxygen and the Co-O bond in the valley configuration are all of the order of 0.46-0.52.

The titanium atoms are also characterized by smaller SBO values than Fe – 2.1 for hill and only 1.8 for valley sites. This matches the binding energies of Ti heteroatoms, because in this case smaller values of the binding energies correspond to the smaller values of SBOs. The values are significantly smaller than the optimal value of 4, thus, the Ti site forms a

potential active site to bind the reactants.

Partial charges

Figure 2 shows the charge density difference occurring upon substitution of an Fe atom with the heteroatoms. For all the investigated cases, the charge redistribution is observed, but it is mostly of a local character, i.e. only the substituted atom and its neighbors are affected.

The smallest and most localized changes are observed for the Co containing system. This holds for both – hill and valley sites, despite the difference in binding energy. Both cobalt and nickel are present on the +2 oxidation state, they bare smaller formal charge than Fe atoms (+3). Partial charges of Co and of Ni also are smaller than those of Fe, and for hill and valley sites they amount to 1.40 and 1.27 (Co) and 1.12 and 1.28 (Ni) respectively. Such a difference in charge is visible in the Figure 2b,c as the yellow area at the substitution site. Contrary to that, the titanium atom is present on the +4 oxidation state and bears a partial charge of 2.32 for hill and 2.01 for the valley sites. As the charge on this atom is higher than the one on Fe, it is visible as the green area in the Figure 2a.

Interestingly, besides the charge redistribution affecting merely the closest neighbors, only the repolarization of the charges is observed on the atoms located in the first two layers. This is confirmed by the DDEC6 charges, especially for Co and Ni systems and the system with Ti in the valley position, where the difference of the charge on the Fe atoms is of the order of 0.01 e. Contrary to that, significant charge difference has been observed for the nearest Fe atom in the system with Ti in the hill site. This is shown in Figure 3(a).

The biggest difference is obviously for the Ti heteroatom, which due to the different oxidation state shows significantly higher charge than Fe. The oxygen atoms in the first coordination sphere are slightly affected, but this is also the case for Co- and Ni- substitutions. The most important observation, however, is the change on the Fe atoms in the second coordination sphere of Ti. The charge on the nearest Fe atom decreased from 1.44 e to 1.10 e, and the SBO from 2.53 to 2.25 (the pure Fe_2O_3 was used as a reference). This

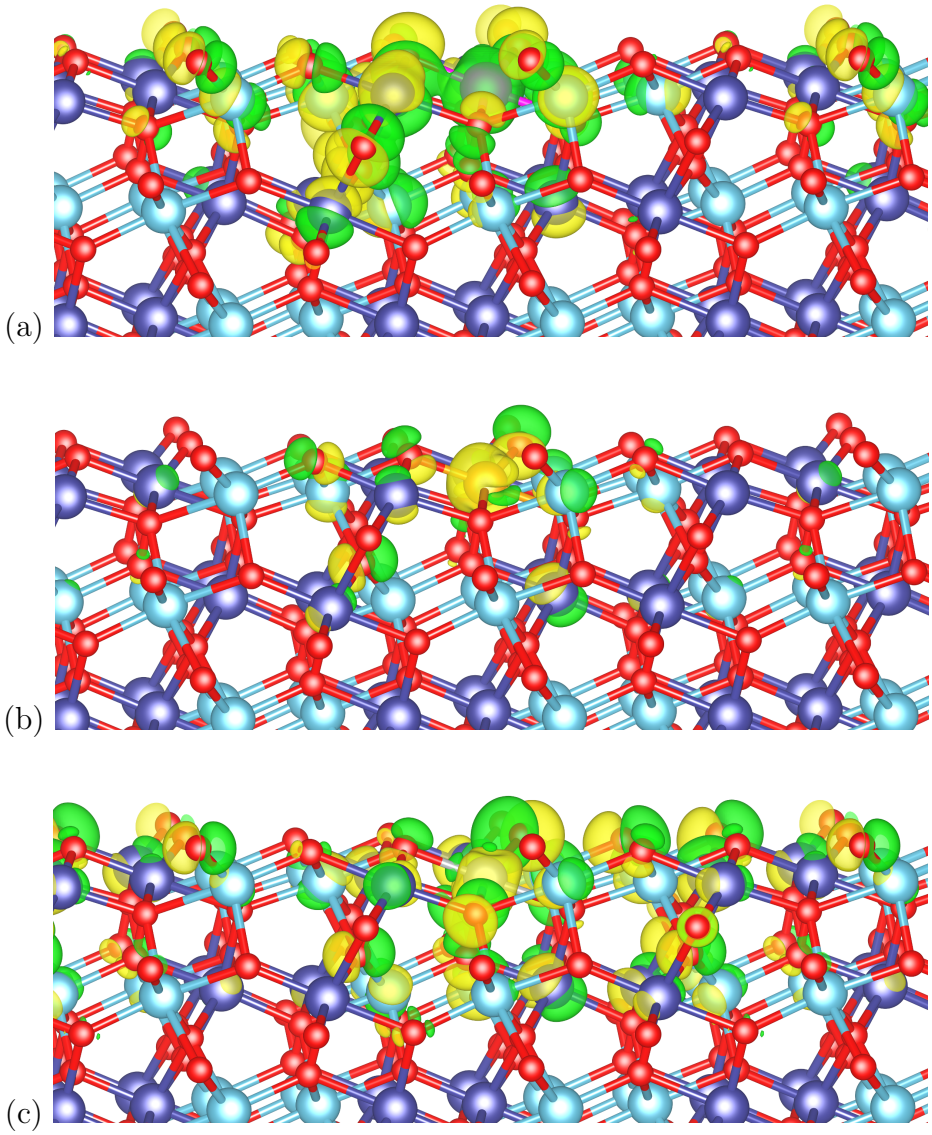

Figure 2: Charge density difference upon substitution of an iron atom with (a) titanium, (b) cobalt and (c) nickel atoms. Dark blue and light blue spheres represent Fe atoms with magnetic moment pointing up and down respectively. Red spheres represent oxygen atoms. Green and yellow colored areas represent accumulation and depletion of the charge respectively. The isosurfaces are drawn for the 0.02 value.

difference is significant enough for the particular Fe atom to behave differently than other surface Fe atoms and potentially act as the active site and due to undercoordination – to stabilize particular surface intermediates.

The changes in charging of these particular sites are also reflected in slight change of the

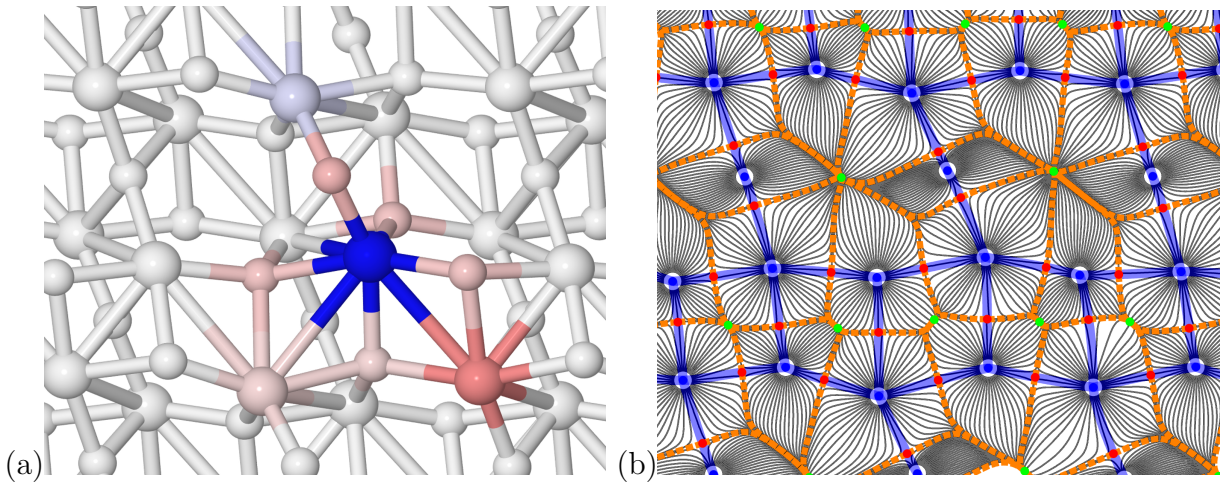

Figure 3: (a) Charge differences caused by the substitution of the hill Fe atom with the Ti. Colors represent the positive (blue) and negative (red) charge difference with respect to the unmodified Fe_2O_3. The darker the shade of blue and red, the more difference in charge is observed. (b) Gradient vector field of electron density for the same system. The red dots denote bond critical points. The positions of atoms are matching in both Figures.

bonding between a subsituted atom and oxygen. Bader analysis classifies bonding interactions into two categories: shared-electron and closed-shell interactions basing on the values of electron density and Laplacian at the bond critical point (BCP), however Cremer and Kraka[69] suggested a more detailed descriptor – the ratio of potential-energy density $|V_c|$ and the kinetic-energy density G_c at the critical point. For Fe_2O_3 all Fe–O bonds are of intermediate character with mostly ionic contribution. That is confirmed by the ratio of potential to kinetic energy at the BCP which is only slightly larger than 1 and varies between 1.071 and 1.275.

For the Ti-system with the substitution in hill-up position, a slight change in the bonding character has been observed. Two out of five Ti-O bonds have the ratio of intermediate value (1.334 and 1.350), what indicates increased covalent character of the bond, however the covalent contribution is still relatively small. Interestingly, the bonds showing increased covalent character are the ones forming the bridges between the Ti and those Fe atoms, whose charge changed the most with respect to the unsubstituted surface. This allows to conclude that the bonding character is responsible for the observed change in charges.

Figure 3(b) shows the atomic basins associated with the Ti/Fe_2O_3 surface layer. The Fe, Ti, 2- and 3-coordinated O atoms can be identified. There is a shift of BCPs on all Ti-O bond-paths towards oxygen atom compared to the Fe-O bond, making the basin for Ti atoms larger. This shift is related to bigger electronegativity of Ti with respect to Fe[70] and is not observed for the other two substitutional atoms (Co and Ni) as they have almost the same electronegativity as Fe (Figure S7). The biggest shift is observed between the Ti atom and 2-coordinated oxygen atom. In addition, the Fe atom displaying the largest charge difference – shown in the brightest shade of red in Figure 3(a) – is also characterized by changed path lines in its basin.

Importantly, the cobalt and nickel substitutions, despite the same formal charge, show differences in the charge distribution at the surface. Clearly, the repolarization of the charges is affecting a larger part of the surface for Ni- than Co-containing system. This is consistent with significant differences in binding energies of Ni and Co in the hill sites as well as the difference in partial charges these atoms are bearing (1.40 e for Co and 1.12 e for Ni). For the valley substitutions, however, Co and Ni show similar pattern – a smaller part of the surface is showing the change in charge density. For these two systems both – the binding energies differ by no more than 0.1 eV and the partial charges by 0.09 e. This is a result of the additional doping states overlapping with the surface states, and more detailed explanation will be discussed in the section on the DOS analysis. A similar pattern is observed for the Ni substituted in the hill site and all Ti-substituted system, despite clear difference in charge on the subatom described above, and significant difference in binding energy of those atoms.

In all the cases, only the atoms (Fe and O) from the top two layers displayed the differences in charge density. The atoms located in the subsequent layers did not show any observable differences. This is consistent with the observation of the different electronic states in the surface and in the bulk discussed in the next section.

Density of states (DOS) analysis

A detailed analysis of the density of states and origin of the peaks observed in the energy gap is complicated by the fact of introduction of the surface and especially – its deformation. This causes many non-equivalent atoms in the surface i.e. located in various chemical environments. This, however, gives only marginally different contributions to DOS. Therefore we focus on the analysis of the similarities and differences of the DOS in surface and bulk geometries.

Using the Fe_2O_3 (110) surface of the rhombohedral cell we obtain a band gap of approximately 1.48 eV, while the gap for bulk geometry in our calculations is 2.10 eV (Figure 4). This narrowing of the band gap is beneficial for the PEC applications, increasing the range of solar energy that can be harvested, but on the other hand, it reduces the redox potential at the surface. Comparing these two values – bulk and surface band gaps – we obtain a difference of approximately 0.6 eV. This is a result of additional surface states, that are not present in the bulk geometry.[71,72]

Table 2 shows the energy gap values for the doped hematite. The energy gap width

Table 2: Values of the energy band gap (in eV) for the surface doped with a subatom with different magnetic moment and position in the unit cell.

		Ti	Co	Ni
hill	$\mu_\downarrow$	1.4	1.5	1.5
	$\mu_\uparrow$	1.5	1.5	1.4
valley	$\mu_\downarrow$	1.5	1.4	1.6
	$\mu_\uparrow$	1.5	1.4	1.6

does not alter significantly upon doping the hematite surface, thus in this geometry the possibility of band gap width modification is limited. This is in contrast to previous findings on narrowing the energy gap in the studies using bulk geometry.[21–23,73] This discrepancy can be explained by the different content of the heteroatoms in those works compared to our model. In the cited papers, in bulk geometry the content of subatoms ranged from a few to about 10%, while in our calculations we use one heteroatom atom per 95 Fe atoms. A direct

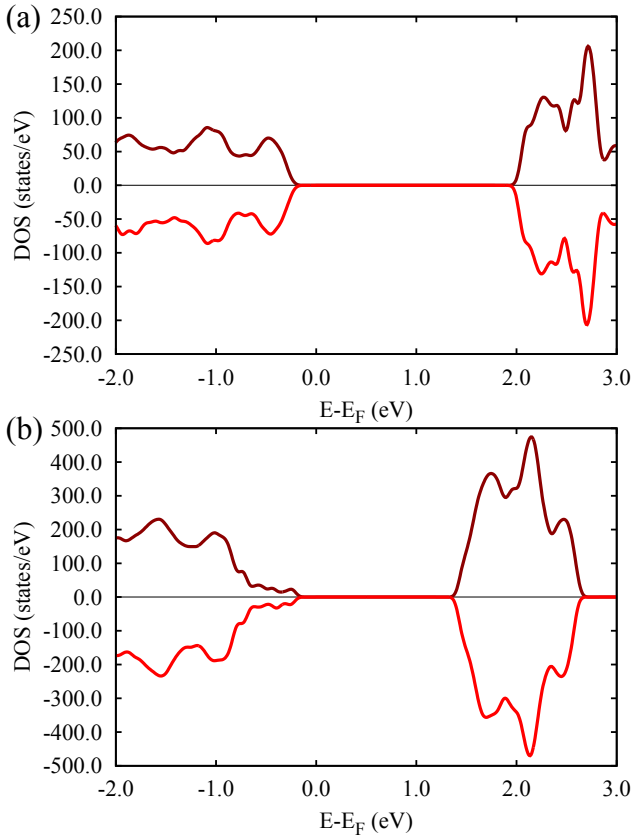

Figure 4: (a) DOS of hematite in bulk geometry. (b) DOS of (110) hematite surface. Positive and negative values of DOS stand for two different directions of magnetic moment.

comparison of the content is difficult due to the differences in the computational models – the weight percent of the heteroatoms amounts to 0.6-0.7 %, but one needs to remember the thickness of our system is chosen arbitrarily, and depending on the thickness the content of the heteroatoms would be higher or lower. On the other hand, a surface coverage of the heteroatoms would not be possible to calculate for the bulk model.

In almost all the cases, substitution of an Fe atom leads to the appearance of additional states in the band gap, but these states are of different character. When an Fe atom is substituted by Ti atom, it leads to the appearance of occupied states (below the Fermi level) in the band gap. This is shown in Figure 5. As Ti has higher oxidation state (+4) than Fe, it becomes a donor.

On the contrary, Co and Ni subatoms show an opposite behavior – both of these species have lower oxidation state (+2) than Fe (+3) and their presence in the system lead to the

formation of the acceptor i.e. unoccupied states in the band gap – see Figure 5. These states, however are located close to the Fermi level, and in the case of Co-substituted system the Co states are overlapping with the surface states in the valence band. As these states are relatively far from the conduction band, we can conclude that their role in the photoactivity of this material will be limited.

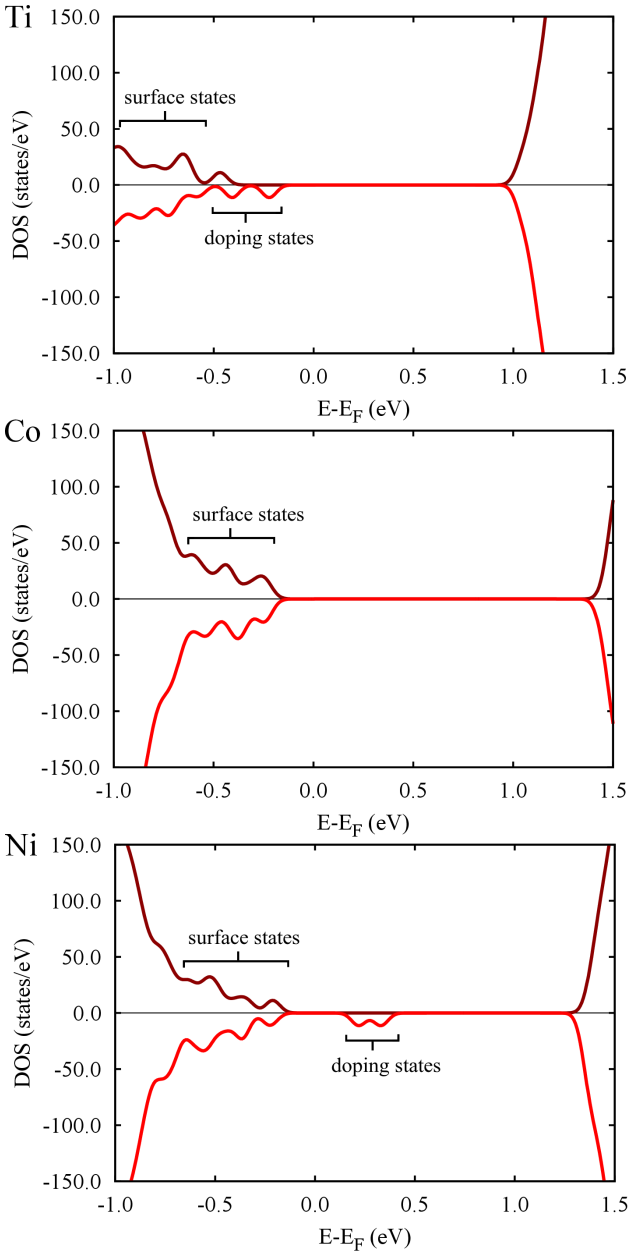

Figure 5: DOS of doped hematite with different substitutional atom in the hill position with magnetic moment up. Positive and negative values of DOS stand for two different directions of spin.

Unexpectedly, in the case of Ti doping, for the valley position of Ti and the magnetic moment down, additional unoccupied state appears in the band gap. A detailed analysis of the density of states shows that the unoccupied state is visible in the spectrum of the atom Ti, but much greater contribution to this state is given by the Fe atoms of the second layer with the magnetic moment directed down. This effect, however, is too subtle to be clearly seen in the charge density plots. Similarly, in the case of nickel doping in the hill position and the magnetic moment down, an occupied state appears in the spectrum. It is mainly associated with the oxygen atoms of the first layer.

Interestingly, a significant difference is observed for the hill and valley Co substitutions, regardless of the magnetic moment. While the Co atoms in the valley positions are associated with acceptor states, in the hill positions – the Co states overlap with the surface states of the Fe_2O_3. These states are below the Fermi level, which means that the Co has changed the oxidation state to +3 when located at the hill site. As Ni does not show such a behavior, we conclude it stays on its formal oxidation state of +2. This coincides with the binding energies shown in Table 1, where Co in the hill position binds more strongly to the surface.

To make a comparison between bulk and surface calculations we present densities of states for both cases – Figures 5 and 6. For the bulk material we have only two possible positions of the substituted atom – i.e. with different magnetic moment directions. There is no difference in the z-coordinate of particular atoms, contrary to the surface. Using substitutional doping we obtain just the same value of the band gap as for pure hematite surface. In each case it is approximately 2.10 eV, however considering the positions of the additional states in the band gap, we can expect it to change for the systems with higher content of the dopant, especially Ti.

We also obtain additional donor and acceptor states in the band gap. It indicates clearly that such a small amount of substitutional atoms cannot significantly influence the width of the band gap. The only difference we obtain are the states in the band gap. Due to these states it is possible to enhance the light absorption, but the small value of their densities

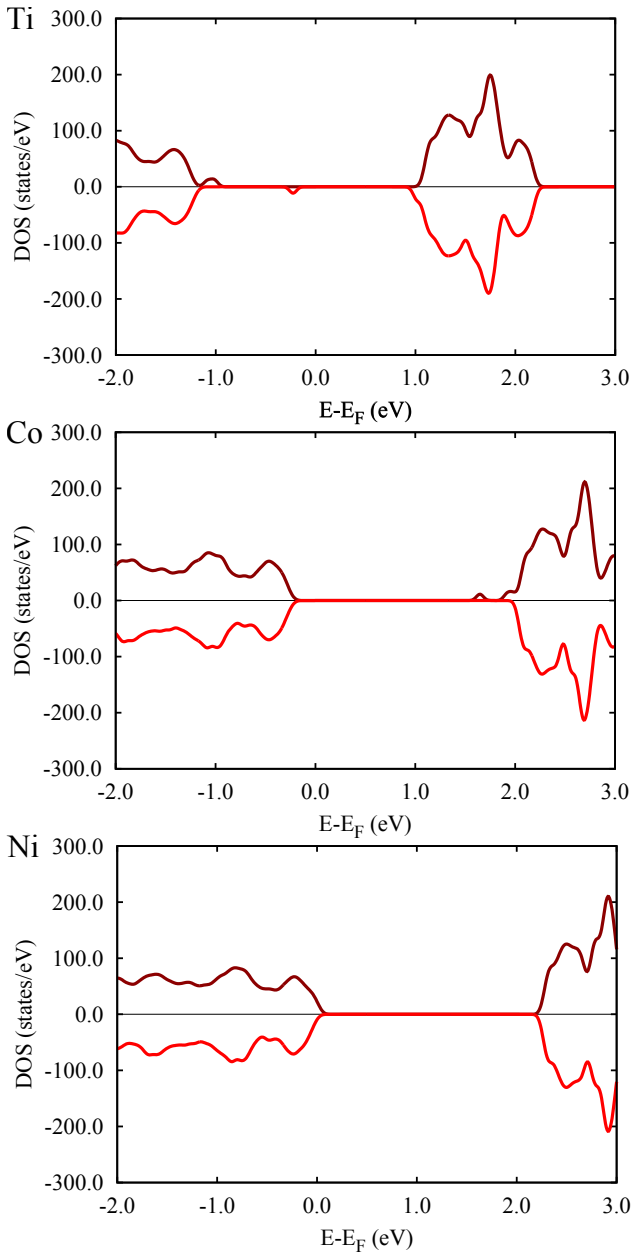

Figure 6: DOS of doped hematite in bulk geometry for one of the magnetic moment direction of a heteroatom. Positive and negative values of DOS stand for two different directions of spin. Due to the symmetry of the system, the densities of states for the heteroatoms magnetic moment of opposite direction are symmetrical.

suggest that this improvement will not be significant.

Lastly, the possibility of the electron/hole traps formation upon doping needs to be mentioned. Because doping states are always localized, there is always an issue of the trapping. On the other hand, the transition takes place between a localized doping state

and a delocalized valence or conduction state. Only if the valence and conduction states were really delocalized, that could restrain the recombination. The problem of hematite are flat bands around the band gap, what means quasi-localized states. In our view, the doping can not significantly influence the rate.

Absorption coefficient

Figure 7 shows the absorption coefficient versus photon energy for pure and doped (110) surface of hematite. To facilitate the analysis of the coefficient, the range of visible light was marked on each graph. It is clear that the absorption coefficient increases when atoms of foreign elements are added. This is related not only to the appearance of additional states in the energy gap but also to the increase of DOS around the gap. It can be noticed, however, that the absorption coefficient increases for photon energies higher than 3 eV, which are in the range of the UV region. The absorption occurs mainly due to the states around the gap and not in the gap. This is of course beneficial, since UV radiation is a part of sunlight, unfortunately irradiation in this range is much lower than for visible light, which is why such an improvement of the absorption coefficient can not significantly increase the efficiency of the electron-hole pair formation.

OER potential

Apart from the absorption study, our goal is to find a proper substrate to study the OER. For this reason, not only the width of the energy gap is important in the research, but also its position relative to the vacuum level. Considering the possibility of water-splitting on different substrates, both potentials need to be taken into account – for hydrogen and oxygen evolution. However, as the focus in this work is the oxygen evolution reactions, only this potential is taken into consideration. The surface of hematite was shown to be suited for application in oxygen evolution reaction in many experimental works.[9–12,74–76]

Table 3 shows the positions of the valence band maximum (VBM) and the conduction

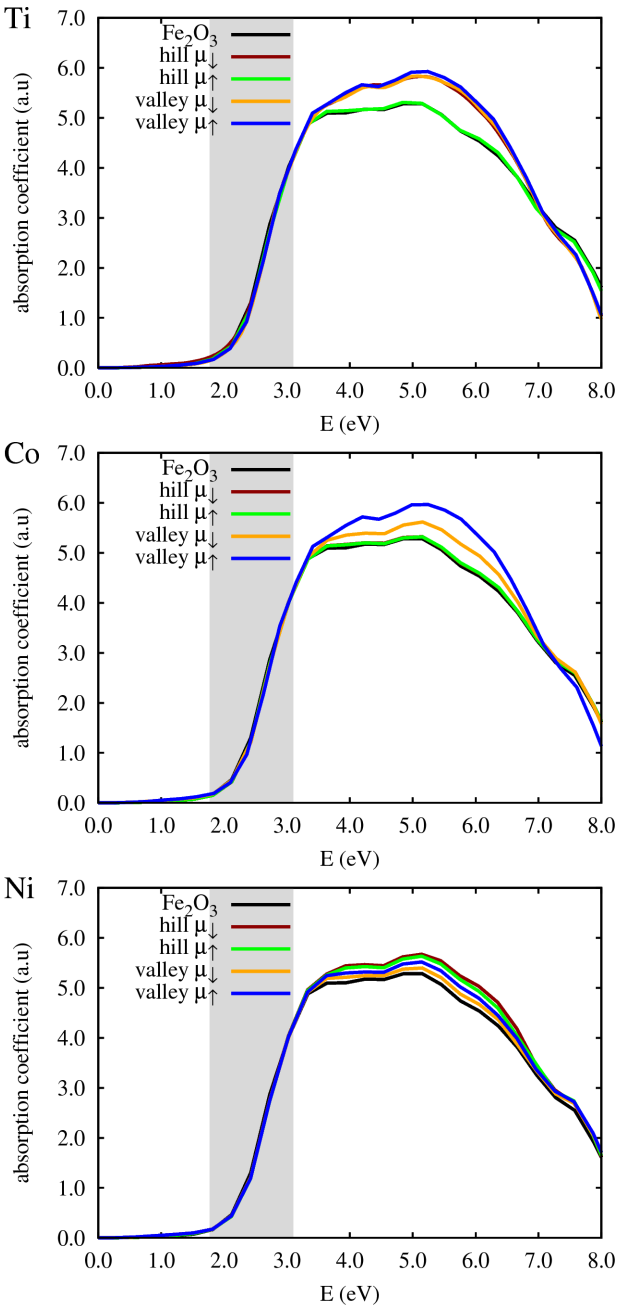

Figure 7: Absorption coefficient of pure and doped hematite surface vs photon energy. Black line labeled as Fe_2O_3 shows the results for the pure surface, the other lines for the doped hematite. The shaded rectangle indicates the visible light region.

band minimum (CBM) related to the vacuum level. For OER, the vacuum potential is -5.67 eV.[77] Comparing this value with VBMs and CBMs in the table, it is clear that for each of the substitution this potential is located inside the energy gap. If we also take into account the binding energy considered above, which indicates the possibility of treating the subatoms

Table 3: Values of VBM and CBM (in eV) of a subatom with different magnetic moment and positions in the unit cell related to the vacuum level 0 eV.

		Ti		Co		Ni	
		VBM	CBM	VBM	CBM	VBM	CBM
hill	$\mu_\downarrow$	-6.93	-5.52	-6.47	-4.98	-6.53	-4.99
	$\mu_\uparrow$	-6.40	-4.91	-6.49	-4.97	-6.55	-5.12
valley	$\mu_\downarrow$	-6.41	-4.95	-6.64	-5.21	-6.69	-5.13
	$\mu_\uparrow$	-6.28	-4.81	-6.62	-5.21	-6.62	-5.02

as the reaction centers, it can be concluded that the use of Ti, Co and Ni as dopants is a promising method for increasing OER efficiency.

Conclusions

We have performed a set of DFT calculations for the (110) surface of the rhombohedral cell of hematite aiming at two main goals. The first one was to show a proper method to perform calculations for both doped and undoped materials used for PEC water-splitting and show how the TM doping influence the energetics and optical properties of the hematite surface. The second one was to improve the hematite surface properties as a template for OER.

We have demonstrated the crucial role of using a correct surface geometry to predict the properties of hematite in the context of its applications in water-splitting. Using only the bulk geometry can be one of the problems of water-splitting research, in particular the discrepancy between the theoretical predictions and the experimental results, because it disregards all surface effects. However useful calculations using bulk geometry are (e.g. allowing to determine the electronic structure in any direction), it should be noted that surface states are critical and not taking into account surface effects by performing calculations in bulk geometry can lead to erroneous conclusions.

We did not achieve any significant improvement in the optical properties of the surfaces – the substitution leads to the increase of the absorption coefficient, but unfortunately this effect occurs for UV radiation, not for visible light. Similarly, the differences observed for

the DOS of a doped and clean surfaces are minor. This is due to a low content of the doping sites, however the position and character of the states coming from the heteroatoms allows to conclude that significant improvement of the optical character of the material due to doping will be unlikely. This is consistent with the experimental results of Hahn and Mullins,[74] where the improvement of the absorption coefficient does not depend on the content of the doping Ti.

Most importantly however, the heterogeneous catalysis is a surface phenomenon, and the doping of the surface atoms will have completely different effect than doping the bulk. So far, the role of a dopant in Fe_2O_3 is little understood, especially in terms of its impact on the electronic structure of the material. In our case, the surface was doped with single atoms of Ti, Co and Ni. Obtained binding energies indicate that each of the proposed dopants can be a suitable co-catalyst in the water-splitting process on the tested surface, however the Ni doping is less likely due to the low binding energy, and the incorporation of this species into the surface will probably occur in a different form.

Each of the investigated dopants display a different mechanisms of action that can be beneficial or disadvantageous for the OER. Nickel's weak binding to the surface is the result of the overcoordination in both hill and valley sites, what is confirmed by the SBO higher than the optimal value of 2 for Ni oxides. Besides that, the heteroatom does not impact the properties of the hematite itself. Cobalt display different characteristics in the hill or the valley configurations – even the small difference of the z-coordinate can lead to the change in the oxidation state of the Co, what is evidenced by the surface states and states of Co atom located below the Fermi level. Titanium, however, impacts the hematite system the most, where the charge decrease of the nearby Fe atom suggests its reduction to Fe^{+2}.

Acknowledgments

BSz and APP acknowledge funding from M-ERA.NET Call 2016 for the project "MuMo4PEC" with project number M-ERA.NET 4089. This work is partially financed by National Centre of Science grant nr. 2016/23/Z/ST4/04376. The simulations have been performed at the Academic Computing Center TASK in Gdańsk, Poznań Supercomputing and Networking Center and Academic Computer Centre Cyfronet in Kraków. This research was supported in part by PL-Grid Infrastructure.

Supporting Information

DOS and charge density difference plots of doped hematite with substitutional atom with different magnetic moment and position in the unit cell, gradient vector field of electron density of undoped and doped hematite.

References

(1) Bard, A. J. Photoelectrochemistry. *Science* **1980**, *207*, 139–144.

(2) Ahmad, H.; Kamarudin, S.; Minggu, L.; Kassim, M. Hydrogen from Photo-Catalytic Water Splitting Process: A Review. *Renewable and Sustainable Energy Reviews* **2015**, *43*, 599 – 610.

(3) Jang, J. S.; Kim, H. G.; Lee, J. S. Heterojunction Semiconductors: A Strategy to Develop Efficient Photocatalytic Materials for Visible Light Water Splitting. *Catalysis Today* **2012**, *185*, 270 – 277, Catalysis on Energy and Environmental Technologies: 13th Korea-Japan Symposium on Catalysis.

(4) Fujishima, A.; Honda, K. Electrochemical Photolysis of Water at a Semiconductor Electrode. *Nature* **1972**, *238*.

(5) Karlsson, R. K.; Cornell, A.; Pettersson, L. G. The Electrocatalytic Properties of Doped TiO_2. *Electrochimica Acta* **2015**, *180*, 514 – 527.

(6) Szyja, B. M.; van Santen, R. A. Synergy Between TiO2 and Co_xO_y Sites in Electrocatalytic Water Decomposition. *Phys. Chem. Chem. Phys.* **2015**, *17*, 12486–12491.

(7) Xu, H.; Zhang, R. Q.; Ng, A. M. C.; Djurišić, A. B.; Chan, H. T.; Chan, W. K.; Tong, S. Y. Splitting Water on Metal Oxide Surfaces. *The Journal of Physical Chemistry C* **2011**, *115*, 19710–19715.

(8) Züttel, A. Hydrogen Storage Methods. *Die Naturwissenschaften* **2004**, *91*, 157–72.

(9) Gilbert, B.; Frandsen, C.; Maxey, E. R.; Sherman, D. M. Band-Gap Measurements of Bulk and Nanoscale Hematite by Soft X-Ray Spectroscopy. *Phys. Rev. B* **2009**, *79*, 035108.

(10) Akl, A. A. Optical Properties of Crystalline and Non-Crystalline Iron Oxide Thin Films Deposited by Spray Pyrolysis. *Applied Surface Science* **2004**, *233*, 307 – 319.

(11) Khan, S. U. M.; Akikusa, J. Photoelectrochemical Splitting of Water at Nanocrystalline n-Fe_2O_3 Thin-Film Electrodes. *The Journal of Physical Chemistry B* **1999**, *103*, 7184–7189.

(12) Glasscock, J.; Barnes, P.; Plumb, I.; Bendavid, A.; Martin, P. Structural, Optical and Electrical Properties of Undoped Polycrystalline Hematite Thin Films Produced Using Filtered Arc Deposition. *Thin Solid Films* **2008**, *516*, 1716 – 1724.

(13) Hankin, A.; Alexander, J. C.; Kelsall, G. H. Constraints to the Flat Band Potential of Hematite Photo-Electrodes. *Phys. Chem. Chem. Phys.* **2014**, *16*, 16176–16186.

(14) Gates, D. M. Spectral Distribution of Solar Radiation at the Earth's Surface. *Science* **1966**, *151*, 523–529.

(15) Kittel, C. *Introduction to solid state physics*; John Willey & Sons, Inc., 1966.

(16) Lin, Y.; Yuan, G.; Sheehan, S.; Zhou, S.; Wang, D. Hematite-Based Solar Water Splitting: Challenges and Opportunities. *Energy Environ. Sci.* **2011**, *4*, 4862–4869.

(17) Pan, H.; Meng, X.; Qin, G. Hydrogen Generation by Water Splitting on Hematite (0001) Surfaces: First-Principles Calculations. *Phys. Chem. Chem. Phys.* **2014**, *16*, 25442–25448.

(18) Tilley, S. D.; Cornuz, M.; Sivula, K.; Grätzel, M. Light-Induced Water Splitting with Hematite: Improved Nanostructure and Iridium Oxide Catalysis. *Angewandte Chemie 122*, 6549–6552.

(19) McFarland, E. W.; Metiu, H. Catalysis by Doped Oxides. *Chemical Reviews* **2013**, *113*, 4391–4427, PMID: 23350590.

(20) Ruiz Puigdollers, A.; Schlexer, P.; Tosoni, S.; Pacchioni, G. Increasing Oxide Reducibility: The Role of Metal/Oxide Interfaces in the Formation of Oxygen Vacancies. *ACS Catalysis* **2017**, *7*, 6493–6513.

(21) Xia, C.; Jia, Y.; Tao, M.; Zhang, Q. Tuning the Band Gap of Hematite α-Fe2O3 by Sulfur Doping. *Physics Letters A* **2013**, *377*, 1943 – 1947.

(22) Kosa, M.; Barad, H. N.; Singh, V.; Keller, D. A.; Shimanovich, K.; Rühle, S.; Anderson, A. Y.; Zaban, A.; Major, D. T. A Combined Computational and Experimental Investigation of Mg Doped α-Fe_2O_3. *Phys. Chem. Chem. Phys.* **2016**, *18*, 781–791.

(23) Huda, M. N.; Walsh, A.; Yan, Y.; Wei, S.-H.; Al-Jassim, M. M. Electronic, Structural and Magnetic Effects of 3d Transition Metals in Hematite. *Journal of Applied Physics* **2010**, *107*, 123712.

(24) Yatom, N.; Neufeld, O.; Caspary Toroker, M. Toward Settling the Debate on the Role of

Fe2O3 Surface States for Water Splitting. *The Journal of Physical Chemistry C* **2015**, *119*, 24789–24795.

(25) Iandolo, B.; Hellman, A. The Role of Surface States in the Oxygen Evolution Reaction on Hematite. *Angewandte Chemie* **2014**, *126*, 13622–13626.

(26) Huang, X.; Ramadugu, S. K.; Mason, S. E. Surface-Specific DFT + U Approach Applied to α-Fe2O3(0001). *The Journal of Physical Chemistry C* **2016**, *120*, 4919–4930.

(27) Hellman, A.; Pala, R. G. S. First-Principles Study of Photoinduced Water-Splitting on Fe_2O_3. *The Journal of Physical Chemistry C* **2011**, *115*, 12901–12907.

(28) Souvi, S. M.; Badawi, M.; Paul, J.-F.; Cristol, S.; Cantrel, L. A DFT Study of the Hematite Surface State in the Presence of H2, H2O and O2. *Surface Science* **2013**, *610*, 7 – 15.

(29) Ovcharenko, R.; Voloshina, E.; Sauer, J. Water Adsorption and O-Defect Formation on Fe2O3(0001) Surfaces. *Phys. Chem. Chem. Phys.* **2016**, *18*, 25560–25568.

(30) Zhang, X.; Klaver, P.; van Santen, R.; van de Sanden, M. C. M.; Bieberle-Hütter, A. Oxygen Evolution at Hematite Surfaces: The Impact of Structure and Oxygen Vacancies on Lowering the Overpotential. *The Journal of Physical Chemistry C* **2016**, *120*, 18201–18208.

(31) Noerpel, M. R.; Lee, S. S.; Lenhart, J. J. X-Ray Analyses of Lead Adsorption on the (001), (110), and (012) Hematite Surfaces. *Environmental Science & Technology* **2016**, *50*, 12283–12291, PMID: 27767293.

(32) Catalano, J.; Fenter, P.; Park, C. Water Ordering and Surface Relaxations at the Hematite (110)–Water Interface. *Geochim. Cosmochim. Acta* **2009**, *73*, 2242–2251.

(33) Toussaint, C.; Le Tran, H. L.; Colson, P.; Dewalque, J.; Vertruyen, B.; Gilbert, B.; Nguyen, N. D.; Cloots, R.; Henrist, C. Combining Mesoporosity and Ti-Doping in

Hematite Films for Water Splitting. *The Journal of Physical Chemistry C* **2015**, *119*, 1642–1650.

(34) Kronawitter, C. X.; Zegkinoglou, I.; Shen, S.-H.; Liao, P.; Cho, I. S.; Zandi, O.; Liu, Y.-S.; Lashgari, K.; Westin, G.; Guo, J.-H. et al. Titanium Incorporation into Hematite Photoelectrodes: Theoretical Considerations and Experimental Observations. *Energy Environ. Sci.* **2014**, *7*, 3100–3121.

(35) Cheng, W.; He, J.; Sun, Z.; Peng, Y.; Yao, T.; Liu, Q.; Jiang, Y.; Hu, F.; Xie, Z.; He, B. et al. Ni-Doped Overlayer Hematite Nanotube: A Highly Photoactive Architecture for Utilization of Visible Light. *The Journal of Physical Chemistry C* **2012**, *116*, 24060–24067.

(36) Saragovi, C.; Arpe, J.; Sileo, E.; Zysler, R.; Sanchez, L. C.; Barrero, C. A. Changes in the Structural and Magnetic Properties of Ni-Substituted Hematite Prepared from Metal Oxinates. *Physics and Chemistry of Minerals* **2004**, *31*, 625–632.

(37) Barrero, C.; Arpe, J.; Sileo, E.; Sánchez, L.; Zysler, R.; Saragovi, C. Ni- and Zn-Doped Hematite Obtained by Combustion of Mixed Metal Oxinates. *Physica B: Condensed Matter* **2004**, *354*, 27 – 34, Proceedings of the Workshop At the Frontiers of Condensed Matter. Magnetism, Magnetic Materials, and their Applications.

(38) Wang, A.; Li, J.; Zhang, T. Heterogeneous Single-Atom Catalysis. *Nat. Rev. Chem.* **2018**, *2*, 65–81.

(39) Fu, Q.; Saltsburg, H.; Flytzani-Stephanopoulos, M. Active Nonmetallic Au and Pt Species on Ceria-Based Water-Gas Shift Catalysts. *Science* **2003**, *301*, 935–938.

(40) Zhang, X.; Shi, H.; Xu, B.-Q. Catalysis by Gold: Isolated Surface Au3+ Ions are Active Sites for Selective Hydrogenation of 1,3-Butadiene over Au/ZrO2 Catalysts. *Angew. Chem. Int. Ed.* **2005**, *44*, 7132–7135.

(41) Hackett, S. F. J.; Brydson, R. M.; Gass, M. H.; Harvey, I.; Newman, A. D.; Wilson, K.; Lee, A. F. High-Activity, Single-Site Mesoporous Pd/Al2O3 Catalysts for Selective Aerobic Oxidation of Allylic Alcohols. *Angewandte Chemie International Edition* **2007**, *46*, 8593–8596.

(42) Kresse, G.; Furthmüller, J. Efficient Iterative Schemes for Ab Initio Total-Energy Calculations Using a Plane-Wave Basis Set. *Phys. Rev. B* **1996**, *54*, 11169–11186.

(43) Kresse, G.; Joubert, D. From Ultrasoft Pseudopotentials to the Projector Augmented-Wave Method. *Phys. Rev. B* **1999**, *59*, 1758–1775.

(44) Perdew, J. P.; Burke, K.; Ernzerhof, M. Generalized Gradient Approximation Made Simple. *Phys. Rev. Lett.* **1996**, *77*, 3865–3868.

(45) Blöchl, P. E. Projector Augmented-Wave Method. *Phys. Rev. B* **1994**, *50*, 17953–17979.

(46) Monkhorst, H. J.; Pack, J. D. Special Points for Brillouin-Zone Integrations. *Phys. Rev. B* **1976**, *13*, 5188–5192.

(47) Dudarev, S. L.; Botton, G. A.; Savrasov, S. Y.; Humphreys, C. J.; Sutton, A. P. Electron-Energy-Loss Spectra and the Structural Stability of Nickel Oxide: An LSDA+U Study. *Phys. Rev. B* **1998**, *57*, 1505–1509.

(48) Mosey, N. J.; Liao, P.; Carter, E. A. Rotationally Invariant Ab Initio Evaluation of Coulomb and Exchange Parameters for DFT+U Calculations. *The Journal of Chemical Physics* **2008**, *129*, 014103.

(49) Rollmann, G.; Rohrbach, A.; Entel, P.; Hafner, J. First-Principles Calculation of the Structure and Magnetic Phases of Hematite. *Phys. Rev. B* **2004**, *69*, 165107.

(50) Arroyo-de Dompablo, M. E.; Morales-García, A.; Taravillo, M. DFT+U Calculations of Crystal Lattice, Electronic Structure and Phase Stability under Pressure of TiO2 Polymorphs. *The Journal of Chemical Physics* **2011**, *135*, 054503.

(51) Deskins, N. A.; Dupuis, M. Electron Transport via Polaron Hopping in Bulk TiO_2: A Density Functional Theory Characterization. *Phys. Rev. B* **2007**, *75*, 195212.

(52) Persson, C.; Ferreira da Silva, A. Strong Polaronic Effects on Rutile TiO2 Electronic Band Edges. *Applied Physics Letters* **2005**, *86*, 231912.

(53) Chen, J.; Wu, X.; Selloni, A. Electronic Structure and Bonding Properties of Cobalt Oxide in the Spinel Structure. *Phys. Rev. B* **2011**, *83*, 245204.

(54) Selcuk, S.; Selloni, A. DFT+U Study of the Surface Structure and Stability of Co3O4(110): Dependence on U. *The Journal of Physical Chemistry C* **2015**, *119*, 9973–9979.

(55) Floris, A.; de Gironcoli, S.; Gross, E. K. U.; Cococcioni, M. Vibrational Properties of MnO and NiO from DFT + U-Based Density Functional Perturbation Theory. *Phys. Rev. B* **2011**, *84*, 161102.

(56) Manz, T. A.; Limas, N. G. Introducing DDEC6 Atomic Population Analysis: Part 1. Charge Partitioning Theory and Methodology. *RSC Adv.* **2016**, *6*, 47771–47801.

(57) Limas, N. G.; Manz, T. A. Introducing DDEC6 Atomic Population Analysis: Part 2. Computed Results for a Wide Range of Periodic and Nonperiodic Materials. *RSC Adv.* **2016**, *6*, 45727–45747.

(58) Manz, T. A. Introducing DDEC6 Atomic Population Analysis: Part 3. Comprehensive Method to Compute Bond Orders. *RSC Adv.* **2017**, *7*, 45552–45581.

(59) Fox, M. *Optical Properties of Solids*; Oxford University Press, 2010.

(60) Henkelman, G.; Arnaldsson, A.; Jónsson, H. A fast and robust algorithm for Bader decomposition of charge density. *Computational Materials Science* **2006**, *36*, 354 – 360.

(61) Yu, M.; Trinkle, D. R. Accurate and efficient algorithm for Bader charge integration. *The Journal of Chemical Physics* **2011**, *134*, 064111.

(62) Bader, R. *Atoms in Molecules: A Quantum Theory*; Clarendon Press, 1994.

(63) D., V.; D., A. AIM-UC: An application for QTAIM analysis. *Journal of Computational Methods in Sciences and Engineering* **2014**, *14*, 131–136.

(64) Sandratskii, L. M.; Uhl, M.; Kübler, J. Band Theory for Electronic and Magnetic Properties of α-Fe_2O_3. *Journal of Physics: Condensed Matter* **1996**, *8*, 983.

(65) Krén, E.; Szabó, P.; Konczos, G. Neutron Diffraction Studies on the (1-x) Fe_2O_3-xRh_2O_3 System. *Physics Letters* **1965**, *19*, 103 – 104.

(66) Szyja, B. M.; Vanpoucke, D. In *Zeolites and Metal-Organic Frameworks From lab to industry*; Vincent Blay, L. F. B., García, A. C., Eds.; Atlantis Press / Amsterdam University Press, 2018.

(67) Ferrer, S.; Rojo, J. M.; Salmerón, M.; Somorjai, G. A. The Role of Surface Irregularities (Steps, Kinks) and Point Defects on the Chemical Reactivity of Solid Surfaces. *Philosophical Magazine A* **1982**, *45*, 261–269.

(68) Aschauer, U.; He, Y.; Cheng, H.; Li, S.-C.; Diebold, U.; Selloni, A. Influence of Subsurface Defects on the Surface Reactivity of TiO2: Water on Anatase (101). *The Journal of Physical Chemistry C* **2010**, *114*, 1278–1284.

(69) Cremer, D.; Kraka, E. Chemical Bonds without Bonding Electron Density — Does the Difference Electron-Density Analysis Suffice for a Description of the Chemical Bond? *Angewandte Chemie International Edition in English* **1984**, *23*, 627–628.

(70) Kumar, A.; Gadre, S. R. Exploring the Gradient Paths and Zero Flux Surfaces of Molecular Electrostatic Potential. *Journal of Chemical Theory and Computation* **2016**, *12*, 1705–1713.

(71) Tamm, I. Some Remarks on the Theory of Photoelectric Effect on Metals. *Phys. Rev.* **1932**, *39*, 170–172.

(72) Shockley, W. *Electrons And Holes In Semiconductors*; Van Nostrand Reinhold Inc.,U.S., 1950.

(73) Pan, H.; Meng, X.; Liu, D.; Li, S.; Qin, G. (Ti/Zr,N) Codoped Hematite for Enhancing the Photoelectrochemical Activity of Water Splitting. *Phys. Chem. Chem. Phys.* **2015**, *17*, 22179–22186.

(74) Hahn, N. T.; Mullins, C. B. Photoelectrochemical Performance of Nanostructured Ti- and Sn-Doped α-Fe2O3 Photoanodes. *Chemistry of Materials* **2010**, *22*, 6474–6482.

(75) Zhang, X.; Li, H.; Wang, S.; Fan, F.-R. F.; Bard, A. J. Improvement of Hematite as Photocatalyst by Doping with Tantalum. *The Journal of Physical Chemistry C* **2014**, *118*, 16842–16850.

(76) Wang, G.; Ling, Y.; Wheeler, D. A.; George, K. E. N.; Horsley, K.; Heske, C.; Zhang, J. Z.; Li, Y. Facile Synthesis of Highly Photoactive α-Fe2O3-Based Films for Water Oxidation. *Nano Letters* **2011**, *11*, 3503–3509, PMID: 21766825.

(77) Tamirat, A. G.; Rick, J.; Dubale, A. A.; Su, W.-N.; Hwang, B.-J. Using Hematite for Photoelectrochemical Water Splitting: A Review of Current Progress and Challenges. *Nanoscale Horiz.* **2016**, *1*, 243–267.

TOC Graphic